

# Equivalent Magnetic Noise in Multi-Push–Pull Configuration Magnetolectric Composites: Model and Experiment

Yaojin Wang, Davresh Hasanyan, Menghui Li, Junqi Gao, Jiefang Li, and Dwight Viehland

**Abstract**—A theoretical model for the multi-push–pull configuration of magnetolectric (ME) laminated composites comprising magnetostrictive and piezoelectric layers with interdigitated electrodes encapsulated in polyimide film is presented. Analytical solutions for the ME voltage coefficient  $\alpha_E$ , ME charge coefficient  $\alpha_Q$ , noise charge density and equivalent magnetic noise were derived. Parametric studies are presented to evaluate the influence of material properties and polyimide film geometries. The results show that the value of  $\alpha_E$  was determined by the parameters of the magnetostrictive and piezoelectric phases, and that the values of  $\alpha_Q$  and noise charge density were determined not only by the component parameters, but also by the volume fraction of the piezoelectric phase and polyimide film geometry. The equivalent magnetic noise had no dependence on the polyimide film geometry, but rather was determined by the component parameters and the volume fraction of the piezoelectric phase. Theoretical and experimental results are compared and shown to have good agreement with each other.

## I. INTRODUCTION

FERROMAGNETISM and ferroelectricity are important phenomena for various technologies. They are at the center of a quest for multiferroic and/or magnetolectric (ME) materials, in which these two phenomena are intimately coupled [1]. The ME effect is characterized by a change in electric polarization in response to an applied magnetic field or, vice versa, a magnetization change in response to an electric field. The ME effect has been observed both in single-phase and composite materials. Until now, more than ten different compound families have been widely investigated as potential multiferroic ME materials, including BiFeO<sub>3</sub> and rare-earth magnets [2], [3]. All single-phase multiferroic materials have a low intrinsic ME coupling at room temperature; thus, potential applications, such as nonvolatile electric-write/magnetic-read memories and spin-wave generators, have not been forthcoming [4].

Composites consisting of magnetostrictive and piezoelectric layers exhibit much larger extrinsic ME effects (e.g., several orders of magnitude) than in single-phase

ones [5], [6]. Accordingly, the ME effect in composites has been an important research topic. Among ME composites, laminates of magnetostrictive Metglas foils (Vacuumscheltze GmbH & Co. KG, Hanau, Germany) and 0.7Pb(Mg<sub>1/3</sub>Nb<sub>2/3</sub>)O<sub>3</sub>–0.3PbTiO<sub>3</sub> (PMN-PT) single-crystal piezofibers operated in a multi-push–pull mode possess the highest ME coefficients [7]. The high property values of their ME laminates open the possibility for their applications as high-sensitivity magnetic field sensors [7]. Numerous experiments have been performed to study the ME properties for various composite configurations, magnetostrictive and piezoelectric phase components [8], and geometrical dimensions [9]. However, their application as magnetic field sensors has, in part, been limited by a lack of theoretical understanding of the ME properties of the multi-push–pull configuration.

Harshe *et al.* proposed a theoretical model for multi-layer heterostructures, with magnetostrictive and piezoelectric layers under various boundary conditions based on piezoelectric and piezomagnetic equations [10]. The ME coefficients in the laminated composite were predicted using the parameters of the magnetostrictive and piezoelectric phase components. Bichurin and Srinivasan obtained a more detailed theoretical model using a field-averaging method [11], [12], which included a coupling factor for the mismatch at the composite bonding interface, which described the strain transfer across the inter-phase interfaces. The coefficients they predicted had similar trends as the experimental data [11]–[13]. Most of the theoretical models of ME composites have so far focused on traditional modes of operation [11], [12], [14], [15]: such as the longitudinal–longitudinal (L-L), and longitudinal–thickness (L-T) modes. Theoretical models for the multi-push–pull have not yet been developed. To realize the full potential of the multi-push–pull mode ME composites for magnetic field sensor applications, such theoretical models for the ME coefficient, noise charge density, and equivalent magnetic noise are important.

Here, we introduce approximate theoretical models for the ME coefficient, noise charge density, and equivalent magnetic noise for a magnetostrictive/piezofiber multi-push–pull configuration. The ME coefficient was obtained using the field-averaging method under the assumption of a uniform polarization direction. Subsequently, for the piezoelectric phase, the dielectric properties of the multi-push–pull configuration were found, and then the noise charge density and equivalent magnetic noise was determined.

Manuscript received April 10, 2012; accepted March 8, 2013. This work was sponsored by the Defense Advanced Research Projects Agency (DARPA).

The authors are with the Department of Materials Science and Engineering, Virginia Polytechnic Institute and State University, Blacksburg, VA (e-mail: yaojin@vt.edu).

DOI <http://dx.doi.org/10.1109/TUFFC.2013.2686>

$$\alpha_{E,33} = \frac{E_3}{H_3} = \frac{\{[{}^m q_{33}({}^p d_{33} {}^p s_{11} - {}^p d_{31} {}^p s_{13}) + {}^m q_{31}({}^p d_{31} {}^p s_{33} - {}^p d_{33} {}^p s_{13})](1-v) + [{}^m q_{33}({}^p d_{33} {}^m s_{33} - {}^p d_{31} {}^m s_{12}) + {}^m q_{31}({}^p d_{31} {}^m s_{33} - {}^p d_{33} {}^m s_{12})]v\}(1-v)}{{}^p \varepsilon_{33}[(1-v)^2({}^p s_{13}^2 - {}^p s_{33} {}^p s_{11}) + (1-v)v(2{}^m s_{12} {}^p s_{13} - {}^m s_{33} {}^p s_{33} - {}^m s_{33} {}^p s_{11}) + v^2({}^m s_{12}^2 - {}^m s_{33}^2)] + (1-v)^2({}^p d_{33}^2 {}^p s_{11} - 2{}^p d_{31} {}^p d_{33} {}^p s_{13} + {}^p d_{31}^2 {}^p s_{33}) + v(1-v)({}^p d_{33}^2 {}^m s_{33} - 2{}^p d_{31} {}^p d_{33} {}^m s_{12} + {}^p d_{31}^2 {}^m s_{33})} \quad (4)$$

## II. THEORETICAL MODELING

### A. General Approach and Assumption

Fig. 1(a) shows a schematic diagram of the multi-push-pull configuration for a Metglas/piezofiber laminate composite. The core composite is composed of a pair of insulating Kapton/interdigitated (ID) electrodes (Kapton, DuPont, Wilmington, DE) with a center-to-center space  $s$  and  $N$  pieces of piezofiber, which was sandwiched by  $n$  layers of Metglas with thicknesses  $t_m$ . The polarization direction of the piezofibers between the adjacent ID electrodes is also illustrated in Fig. 1(a). We consider the thickness ( $t_p$ ) of the core composite as being totally contributed by the piezofiber, as the thicknesses of the bonding epoxy and Kapton are negligible compared with  $t_p$ . Analysis assumed that the polarization of piezofibers was uniformly arranged along the longitudinal direction (3-axis). Thus, the multi-push-pull configuration can be considered as a multi-L-L mode, as illustrated in Fig. 1(b). Correspondingly, the simplified configuration consisted of numerous alternating symmetric L-L mode units in a parallel electrical connection, each of length  $s$ . Although the derivation is specific to this layout, the approach is valid for any other type of multi-push-pull configuration.

For a poled piezoelectric phase with the symmetry  $\infty m$ , the constitutive equations for the strain and electric displacement can be written as

$$\begin{aligned} {}^p S_i &= {}^p s_{ij} {}^p T_j + {}^p d_{ki} {}^p E_k \\ {}^p D_k &= {}^p d_{ki} {}^p T_i + {}^p \varepsilon_{kn} {}^p E_n, \end{aligned} \quad (1)$$

where  ${}^p S_i$  and  ${}^p T_j$  are the strain and stress tensor components of the piezoelectric phase;  ${}^p E_k$ ,  ${}^p E_n$ , and  ${}^p D_k$  are the vector components of the electric field and electric displacement;  ${}^p s_{ij}$  and  ${}^p d_{ki}$  are the compliance and piezoelectric coefficients; and  ${}^p \varepsilon_{kn}$  is the permittivity tensor matrix of the piezoelectric phase. The magnetostrictive phase was assumed to have a cubic symmetry, and can be described by the following constitutive equations:

$$\begin{aligned} {}^m S_i &= {}^m s_{ij} {}^m T_j + {}^m q_{ki} {}^m H_k \\ {}^m B_k &= {}^m q_{ki} {}^m T_i + {}^m \mu_{kn} {}^m H_n, \end{aligned} \quad (2)$$

where  ${}^m S_i$  and  ${}^m T_j$  are the strain and stress tensor components of the magnetostrictive phase;  ${}^m H_k$ ,  ${}^m H_n$ , and  ${}^m B_k$  are the vector components of the magnetic field and magnetic flux induction;  ${}^m s_{ij}$  and  ${}^m q_{ki}$  are the compliance and

piezomagnetic coefficients; and  ${}^m \mu_{kn}$  is the permeability matrix of the magnetostrictive phase.

### B. ME Coefficients

Our analysis assumed small deformations, linear material properties, perfect interfacial bonding, and open-circuit condition. For the solutions of (1) and (2), the following boundary conditions of a traction-free plane stress in the cross-sectional directions, equivalence of in-plane strains and equilibrium were used, yielding

$$\begin{aligned} {}^m S_i &= {}^p S_i, \quad (i = 1, 3), \\ {}^m T_2 &= {}^p T_2 = 0, \\ (1 - \nu) {}^m T_i + \nu {}^p T_i &= 0, \quad (i = 1, 3), \\ {}^p D_3 &= 0, \end{aligned} \quad (3)$$

where  $\nu = t_p/(t_p + 2t_m)$  denotes the thickness fraction of the piezoelectric phase.

The constitutive equations can then be solved to predict the uniform (or far-field) ME coefficient under an applied magnetic field based on the nonzero parameters for the magnetostrictive/piezoelectric phases, given (4), see above.

The expression for the ME coefficient in each single unit corresponds to a special case of Bichurin's theory assuming  $k = 1$  [11]. The model considered here then leads to an expression for the multi-push-pull configuration ME coefficient, allowing its estimation as a function of volume fraction and material parameters. In particular, the ME coefficient of this structure was determined not only by the longitudinal-extensional mode piezoelectric coefficient  $d_{33}$ , but also by the transverse-extensional mode piezoelectric coefficient  $d_{31}$ , because the mediated strains were considered in both 1 and 3 directions. A detailed discussion of the theory and its application to the equivalent magnetic noise will be presented in Section III.

The ME voltage coefficient  $\alpha_V$  in a sensor unit can then be determined by  $\alpha_E$  and the space  $s$  between ID electrodes (i.e.,  $\alpha_V = s\alpha_E$ ). Because the laminate consisted of  $m$  ( $m = L/s$ , where  $L$  is the length of the piezofiber) units of electrical polarization in a parallel connection, the ME charge coefficient  $\alpha_Q$  for the multi-push-pull mode laminate composite can be given as

$$\alpha_Q = \frac{{}^p \varepsilon_{33} \alpha_E V}{s}, \quad (5)$$

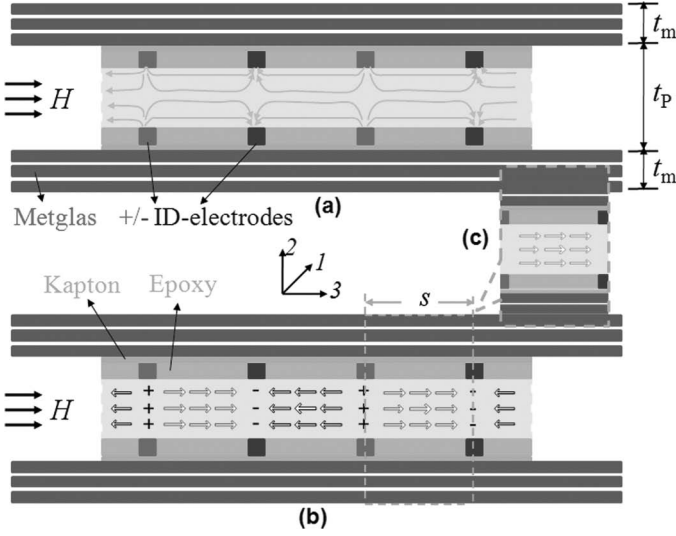


Fig. 1. (a) Schematic diagram of the Metglas/piezofiber multi-push-pull mode configuration consisting of a Kapton/piezofiber core composite and symmetric  $n$ -layer Metglas actuators on the bottom and top of the core composite, where the polarization of piezoelectric and the dead zone are illustrated. The Kapton consisted of interdigitated electrodes and insulating polymer Kapton, which was bonded to the piezofiber by an epoxy resin. (b) Schematic diagram of the simplified multi-L-L-mode structure, in which the polarization of piezofibers was idealized to be arranged in the longitudinal direction over the entire center-to-center distance ( $s$ ) of adjacent ID electrodes. (c) This simplified structure has numerous alternating symmetric longitudinal poled L-L-mode units in an electrically-parallel-connection.

where  $V$  is the volume of the piezofibers ( $V = L \times A$ , where  $A$  is the cross-sectional area of the piezofibers). We can see that  $\alpha_Q$  for the multi-push-pull mode is proportional to the volume of the piezofibers, and inversely proportional to the space of the ID electrodes.

### C. Noise Charge Density

The dominate contributions to the equivalent magnetic noise of ME laminate comes from sources internal to the sensor: namely the dielectric loss ( $N_{DE}$ ) and dc leakage resistance ( $N_R$ ) noises [7], [16]. Please note that the secondary noise sources such as electrical circuit, thermal, and magnetic noise were ignored in this study [16]–[19]. The total noise charge density from these two most significant noise sources can be estimated as [7], [16]:

$$\begin{aligned} N_t \text{ (C}/\sqrt{\text{Hz}}) &= \sqrt{N_{DE}^2 + N_R^2} \\ &= \sqrt{\frac{4kTC_p \tan \delta}{2\pi f} + \frac{1}{(2\pi f)^2} \frac{4kT}{R_{dc}}}; \end{aligned} \quad (6)$$

where  $k$  is Boltzmann's constant ( $1.38 \times 10^{-23}$  J·K<sup>-1</sup>),  $T$  is the temperature in kelvin,  $C_p$  is the capacitance,  $\tan \delta$  is the dielectric loss,  $R_{dc}$  is the dc resistance, and  $f$  is the frequency in hertz.

The value of  $C_p$  for the sensor can be determined from the capacitance of one unit and the number of units [i.e.,  $C_p = ({}^p\varepsilon_{33} V)/s^2$ ], and the total dielectric loss is the same as  $\tan \delta$  of one unit. The value of  $R_{dc}$  of a sensor is the

sum values of  $m$  units in parallel electrical connection [i.e.,  $R_{dc} = (\rho s^2)/V$ , where  $\rho$  is the dc resistivity]. Inputting the corresponding parameters into (6), the total noise charge density ( $N_C$ ) can be re-expressed as

$$N_C \text{ (C}/\sqrt{\text{Hz}}) = \frac{1}{s} \sqrt{\frac{4kT \tan \delta {}^p\varepsilon_{33} V}{2\pi f} + \frac{1}{(2\pi f)^2} \frac{4kTV}{\rho}}. \quad (7)$$

### D. Equivalent Magnetic Noise

The equivalent magnetic noise can then be obtained from the value of  $\alpha_Q$  for the sensor and the total noise charge density [16], given as

$$\begin{aligned} \text{Equivalent magnetic noise (T}/\sqrt{\text{Hz}}) &= \frac{N_C \text{ (C}/\sqrt{\text{Hz}})}{\alpha_Q \text{ (C/T)}} = \frac{\sqrt{\frac{4kT \tan \delta {}^p\varepsilon_{33} V}{2\pi f} + \frac{1}{(2\pi f)^2} \frac{4kTV}{\rho}}}{{}^p\varepsilon_{33} \alpha_E}. \end{aligned} \quad (8)$$

It is important to note that the equivalent magnetic noise of the multi-push-pull mode was independent of the spacing of the ID electrodes, and inversely proportional to the square root of the volume of piezofibers in the laminates. These predictions will be experimentally validated in Section III.

## III. RESULTS AND DISCUSSION

The preceding theoretical model then allowed for a detailed analysis of the ME effect in multi-push-pull configuration laminated composites. Analysis was first done on the influence of the thickness fraction  $v$  of the piezoelectric components on the ME coefficients. The predicted ME voltage coefficient  $\alpha_E$  for the Metglas/PZT-fiber composites given in Fig. 2(a) were obtained assuming non-demagnetization and non-shear lag effects [14], using the material parameters given in Table I. Obviously, ME coupling effects were absent in the individual phase ( $v = 0$ , magnetostrictive;  $v = 1$ , piezoelectric). As  $v$  was increased from  $0 < v < 1$ , the value of  $\alpha_E$  reached a maximum value of 26.5 V/cm·Oe at  $v = 0.51$ : this maximum was due to an increased elastic interaction between piezoelectric and magnetostrictive layers [15]. The value of  $\alpha_E$  then decreased with a further increase of  $v$ . These predicted values were consistent with experimental observations [11], [15]. Experimentally, the dependence of  $\alpha_E$  on  $v$  was measured by stacking  $N$  layers of Metglas on both sides of the PZT-fibers with  $s = 1$  mm. Inspection of Fig. 2(a) will reveal similar trends between predicted and measured values. The maximum measured value of  $\alpha_E$  was 21.5 V/cm·Oe at  $v_m = 0.53$ , which was slightly higher than the predicted value. This slight difference may be due to over-assumptions of non-demagnetization, non-shear lag, and perfect interfaces [11], [14], [15]. The shift in the observed maximum  $\alpha_E$  to higher values of  $v$  toward higher fractions of the piezoelectric phase, relative to predicted ones, may

TABLE I. MATERIAL PARAMETERS FOR MAGNETOSTRICTIVE AND PIEZOELECTRIC COMPONENTS IN THE MULTI-PUSH-PULL CONFIGURATION.

Parameter (units)		Metglas <sup>a</sup>	PZT <sup>b</sup>
Piezoelectric constant ( $10^{-12}$ C/N)	$d_{31}$		-185
	$d_{33}$		440
Piezomagnetic coefficient <sup>c</sup> ( $10^{-9}$ m/A)	$q_{31}$	-21.3	
	$q_{33}$	50.3	
Dielectric constant	$p\varepsilon_{33}/\varepsilon_0$		1750
Elastic compliance ( $10^{-12}$ m <sup>2</sup> /N)	$p s_{11}$		15.3
	$p s_{13}$		-5
	$p s_{33}$		17.3
	$m s_{12}$	-5.2	
	$m s_{33}$	10	
Dielectric loss	$\tan\delta$		0.012
dc resistivity <sup>c</sup> ( $10^8$ $\Omega\cdot\text{m}$ )	$\rho$		30

<sup>a</sup>Cited from [22].

<sup>b</sup>Cited from [11].

<sup>c</sup>Measured value.

result from a non-continuous alteration of the Metglas thickness and a less than perfect interfacial coupling [15].

The variations between predicted and measured values of  $\alpha_E$  with ID electrode spacing  $s$  are shown in Fig. 2(b). It can be seen that  $\alpha_E$  was predicted to be independent of  $s$ , and to be only dependent on the material parameters of the component phases. However, the measured values of  $\alpha_E$  for  $s = 1, 1.8,$  and  $2.5$  mm were 21.5, 13.9, and 11.2 V/cm·Oe, which were factors of 1.2 times, 1.9 times, and 2.4 times smaller than the predicted ones. It is important to note that the poling voltages for these three laminates were 1600, 2000, and 2400 V, respectively. For  $s = 2.5$  mm, the applied voltage may be higher than the dielectric breakdown strength because of residual bubbles between bonding Kapton and PZT-fibers in the laminate. Because of the reduced poling voltages for large ID electrode spacings, the PZT-fibers might have lower piezoelectric properties, which correspondingly reduce  $\alpha_E$ .

Fig. 3(a) shows the values of  $\alpha_Q$  for Metglas/PZT-fiber laminates with ID electrode spacings of  $s = 1, 1.8,$  and  $2.5$  mm, which were calculated using (5). The core composites consisted of 5 PZT-fibers ( $N = 5$ ), each with dimensions of  $40 \times 2 \times 0.2$  mm. It can be seen that the change in the predicted values of  $\alpha_Q$  with  $s$  as a function of  $v$  had the same trends as that in  $\alpha_E$ . The maximum values of  $\alpha_Q$  for  $s = 1, 1.8,$  and  $2.5$  mm were 3470, 1928, and 1388 pC/Oe, respectively: an obvious decrease with increasing  $s$ . The corresponding experimental data for  $s = 1$  mm are also plotted in Fig. 3(a). It can be seen that the measured values of  $\alpha_Q$  followed trends similar to the predicted values, with a maximum value at  $v_m = 0.53$ . Furthermore, both predicted and measured values of  $\alpha_Q$  decreased with increasing  $s$ . The measured values for  $s = 1, 1.8,$  and  $2.5$  mm were 1402, 985, and 915 pC/Oe, respectively: which are factors of 2.48 times, 1.96 times, and 1.52 times smaller than the predicted values. These differences between predicted and measured values of  $\alpha_Q$  for various ID electrode spacing can be attributed to differences between predicted and measured values of the capacitance  $C$ .

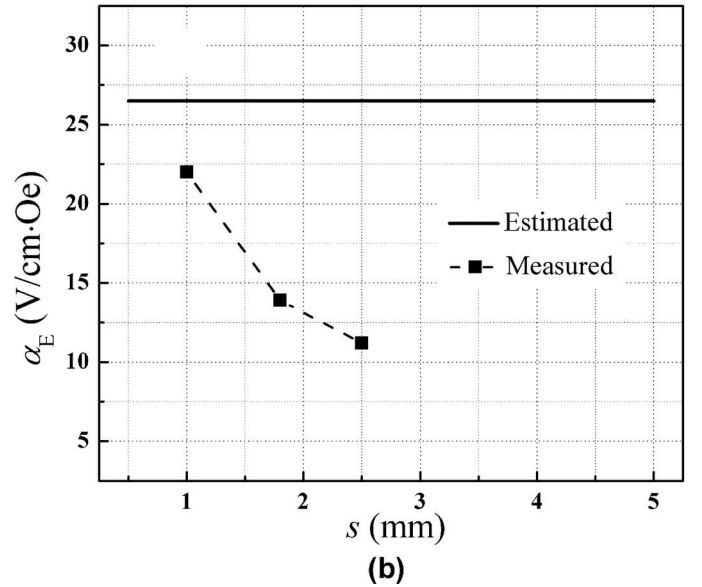
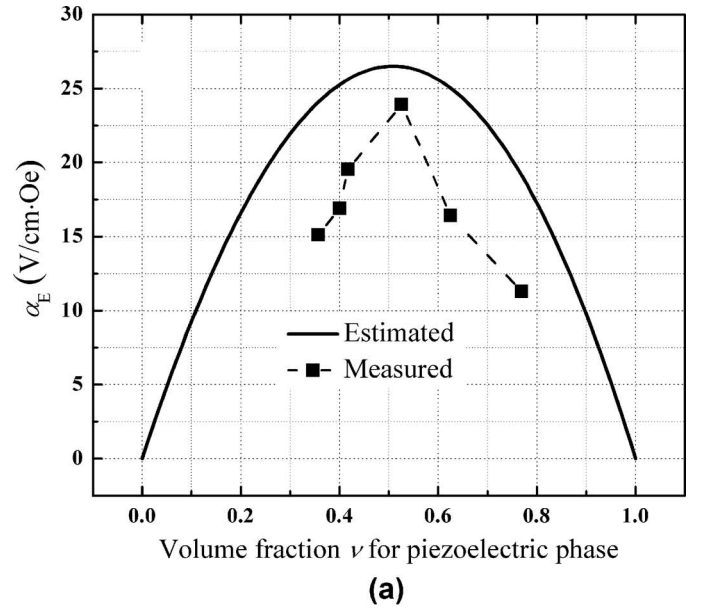


Fig. 2. (a) Estimated and measured values of  $\alpha_E$  for multi-push-pull configuration Metglas/PZT-fiber composite as a function of the volume fraction  $v$  of the PZT-fibers phase. (b) Estimated and measured maximum of  $\alpha_E$  (at optimal  $v$  dependence) as a function of the ID electrodes spacing  $s$  of the Kapton over the range of  $0.5 \text{ mm} < s < 5 \text{ mm}$ .

Accordingly, the capacitance and dc resistance of the laminates was next studied as a function of the ID electrode spacing, as given in the inset of Fig. 3(b). The capacitance decreased with increasing  $s$ , whereas the dc resistance increased. The measured capacitance values for  $s = 1, 1.8,$  and  $2.5$  mm were 472, 248, and 181 pF: which were factors of 2.77 times, 1.63 times, and 1.15 times smaller than the predicted values. It is obvious that the proportional relationship between predicted and measured values of  $C$  can be estimated from those of  $\alpha_E$  and  $\alpha_Q$ . This large difference between predicted and measured values of  $\alpha_Q$  and/or  $C$  at small ID electrode spacing might be due to an oversimplification of the theoretical model with

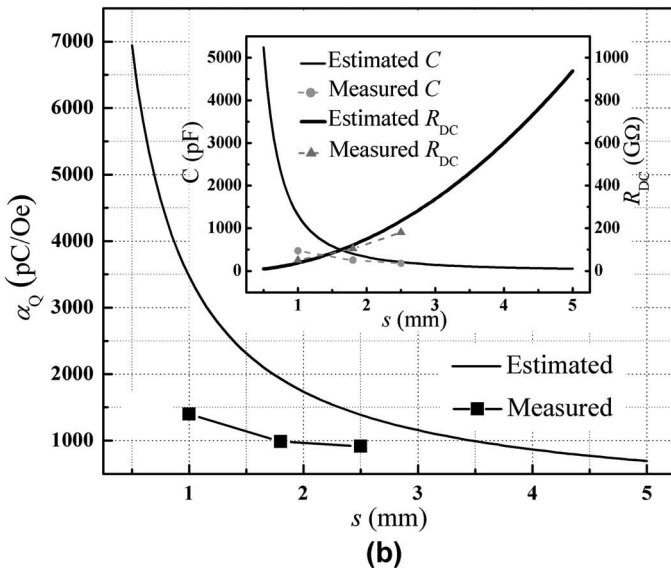
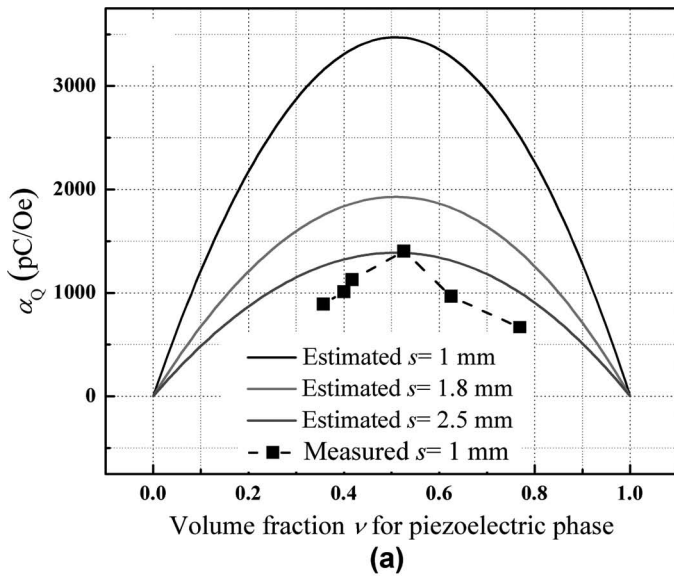


Fig. 3. (a) Estimated and measured values of  $\alpha_Q$  for a multi-push-pull configuration Metglas/PZT-fiber composite as a function of the volume fraction  $\nu$  of the PZT-fiber phase. (b) Estimated and measured maximum  $\alpha_Q$  (at optimal  $\nu$  dependence) on the  $s$  of Kapton over the range of  $0.5 \text{ mm} < s < 5 \text{ mm}$ . The inset shows the theoretical and experimental values of  $C$  and  $R_{dc}$  as a function of  $s$ .

regard to a uniform polarization direction and a non-dead zone in the PZT-fiber [20]. Furthermore, from the inset, we can see the measured dc resistances for  $s = 1, 1.8,$  and  $2.5 \text{ mm}$  were  $50, 108,$  and  $180 \text{ G}\Omega$ : which were close to the predicted resistances.

Fig. 4(a) shows the predicted and measured charge noise density for a Metglas/PZT-fiber sensor unit with  $s = 1 \text{ mm}$  in the frequency range of  $0.125 < f < 100 \text{ Hz}$ . The charge noise density, resulting from contributions of  $\tan \delta$  and dc resistance, was modeled based on (7) using parameters listed in Table I. At the frequency of  $f = 1 \text{ Hz}$ , which is of interest to magnetic sensors, both the  $\tan \delta$  and dc resistance noises contributed to the total noise floor, but the magnitude of the  $\tan \delta$  noise contribution was a factor

of 2 times larger than that of the dc resistance contribution. From (7), we can see that the predicted value of the total noise charge density was determined not only by the material parameters of the Metglas and PZT fibers, but also by the ID electrode spacing of the Kapton, as can also be seen in Fig. 4(b). Similar trends were observed between the predicted and experimental noise charge density as a function of  $s$ . The measured values of the noise charge density for  $s = 1, 1.8,$  and  $2.5 \text{ mm}$  were  $0.168, 0.124,$  and  $0.114 \text{ fC}/\sqrt{\text{Hz}}$ , respectively. In this figure, it can also be seen that the experimental noise charge density (for  $s = 1 \text{ mm}$ ) was higher than the predicted one; however the experimental value for  $s = 2.5 \text{ mm}$  was smaller than the predicted value; Again, we attribute this difference to an oversimplification of the theoretical model with regards to

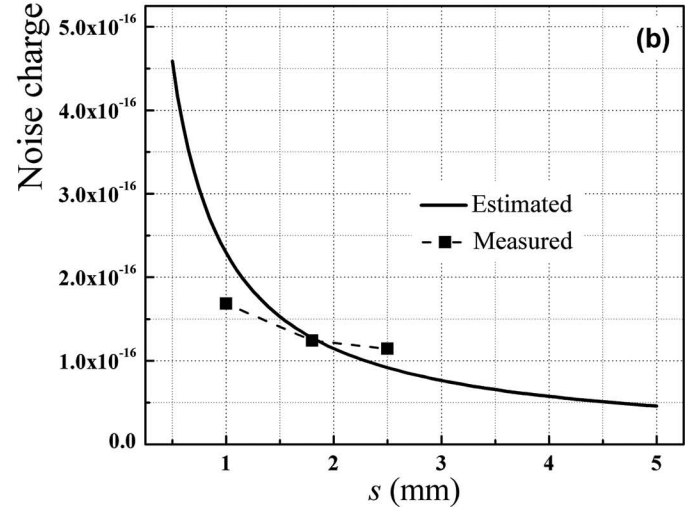
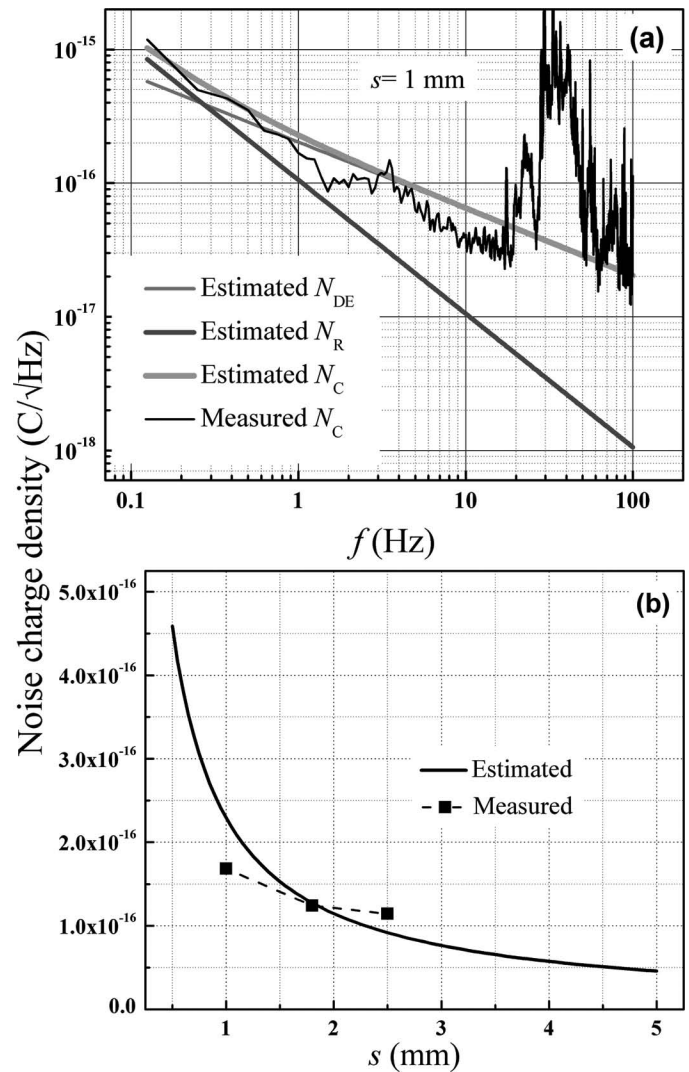


Fig. 4. (a) Estimated and measured charge noise density of a Metglas/PZT-fiber sensor unit, including constituent dielectric loss and dc resistance loss contributions, over the frequency range of  $0.125 \text{ Hz} < f < 100 \text{ Hz}$  for  $s = 1 \text{ mm}$ . The modeling results show that the dc resistance noise is dominant below  $0.25 \text{ Hz}$ . At a frequency of  $f = 1 \text{ Hz}$ , which is of interest to magnetic sensors, the total charge noise density was dominated by the dielectric loss noise. (b) Theoretical charge noise density as a function of  $s$  and the experimental data for a Metglas/PZT-fiber sensor.

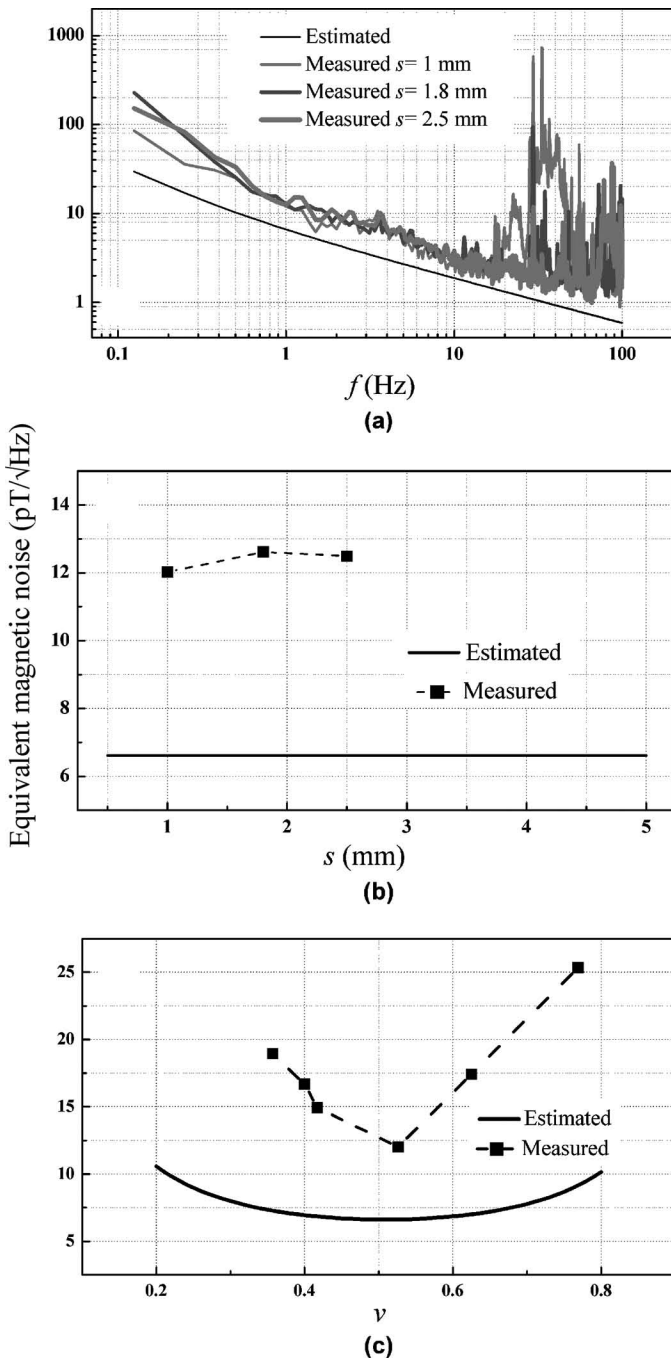


Fig. 5. (a) Predicted and measured equivalent magnetic noise over the frequency range of  $0.125 \text{ Hz} < f < 100 \text{ Hz}$ . The experimental equivalent magnetic noise for  $s = 1, 1.8,$  and  $2.5 \text{ mm}$  are given. (b) Predicted and measured  $1 \text{ Hz}$  equivalent magnetic noise as a function of the ID electrodes spacing  $s$  of Kapton, that was obtained from (a), which shows no dependence on  $s$ . (c) Predicted  $1 \text{ Hz}$  equivalent magnetic noise as a function of the PZT-fiber thickness ratio  $v$ , and the experimental data for  $s = 1 \text{ mm}$ .

a uniform polarization direction and a non-dead zone in the PZT-fiber [20].

Fig. 5(a) shows the predicted and measured values of the equivalent magnetic noise (in  $\text{pT}/\sqrt{\text{Hz}}$ ), which was obtained through a conversion of the charge noise density and the ME charge coefficient [16]. Please note that the values of  $\alpha_Q$  for such heterostructure are maintained

down to quasi-static frequencies [7], [21]. Except at frequencies where external vibration sources are present, the predicted and measured equivalent magnetic noises have the same trends. On the basis of (8), it can be predicted that the equivalent magnetic noise should have no dependence on the ID electrode spacing of Kapton, see in Fig. 5(b). The predicted  $1 \text{ Hz}$  equivalent magnetic noise was  $6.6 \text{ pT}/\sqrt{\text{Hz}}$ ; whereas the measured  $1 \text{ Hz}$  equivalent magnetic noises for  $s = 1, 1.8,$  and  $2.5 \text{ mm}$  were close to  $12 \text{ pT}/\sqrt{\text{Hz}}$ . This difference between predicted and measured equivalent magnetic noises resulted from differences in the ME charge coefficient and noise charge density, as discussed in reference to Figs. 3(b) and 4(b). Finally, the dependence of the equivalent magnetic noise on the PZT-fiber thickness fraction  $v$  is shown in Fig. 5(c). It was obvious that  $v$  was predicted to have little influence on the noise charge density; however,  $v$  affects the value of  $\alpha_Q$ . Thus, the equivalent magnetic noise is dependent on  $v$ , via  $\alpha_Q$ . Please note that the sensor exhibited the lowest predicted and measured equivalent magnetic noises at  $v_m = 0.53$ , near which value of  $\alpha_Q$  was highest.

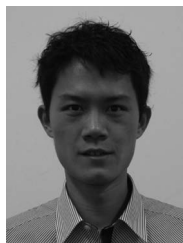
#### IV. CONCLUSIONS

A theoretical model has been developed for the low-frequency ME effect, noise charge density, and equivalent magnetic noise of multi-push-pull configurations of magnetostrictive/piezofiber laminates. Material parameters and geometry were capable of predicting the values for these properties. Theory predicted a giant ME coefficient of  $26.5 \text{ V}/\text{cm}\cdot\text{Oe}$  and an extremely low equivalent magnetic noise of  $6.6 \text{ pT}/\sqrt{\text{Hz}}$  for a laminate design consisting of Metglas and PZT-fibers. In general, the dielectric loss is the principal noise contribution above  $f = 0.25 \text{ Hz}$ , and is a factor of 2 times larger than that of the dc resistance noise at  $f = 1 \text{ Hz}$ . Analytical predictions for the ME coefficients, noise charge density, and equivalent magnetic noise were also compared with experimental data. This comparison yielded good agreement of the ME voltage coefficients and equivalent magnetic noises; however, the predicted and measured values of  $\alpha_Q$  on ID electrode spacing were not as good, probably because of an oversimplification of the theoretical model.

#### REFERENCES

- [1] N. A. Spaldin and M. Fiebig, "The renaissance of magnetoelectric multiferroics," *Science*, vol. 309, pp. 391–392, Jul. 2005.
- [2] S. W. Cheong and M. Mostovoy, "Multiferroics: A magnetic twist for ferroelectricity," *Nat. Mater.*, vol. 6, pp. 13–20, Jan. 2007.
- [3] Z. X. Cheng, X. L. Wang, S. X. Dou, H. Kimura, and K. Ozawa, "Improved ferroelectric properties in multiferroic  $\text{BiFeO}_3$  thin films through La and Nb codoping," *Phys. Rev. B*, vol. 77, art. no. 092101, Mar. 2008.
- [4] C. Israel, N. D. Mathur, and J. F. Scott, "A one-cent room-temperature magnetoelectric sensor," *Nat. Mater.*, vol. 7, pp. 93–94, Feb. 2008.
- [5] J. Ma, J. Hu, Z. Li, and C.-W. Nan, "Recent progress in multiferroic magnetoelectric composites: From bulk to thin films," *Adv. Mater.*, vol. 23, no. 9, pp. 1062–1087, 2011.

- [6] C. W. Nan, M. I. Bichurin, S. X. Dong, D. Viehland, and G. Srinivasan, "Multiferroic magnetoelectric composites: Historical perspective, status, and future directions," *J. Appl. Phys.*, vol. 103, art. no. 031101, Feb. 2008.
- [7] Y. J. Wang, D. Gray, D. Berry, J. Q. Gao, M. H. Li, J. F. Li, and D. Viehland, "An extremely low equivalent magnetic noise ( $\sim$ pT Hz $^{-1/2}$ ) magnetoelectric sensor," *Adv. Mater.*, vol. 23, no. 35, pp. 4111–4114, 2011.
- [8] J. Gao, J. Das, Z. Xing, J. Li, and D. Viehland, "Comparison of noise floor and sensitivity for different magnetoelectric laminates," *J. Appl. Phys.*, vol. 108, no. 8, art. no. 084509, 2010.
- [9] J. Das, J. Gao, Z. Xing, J. F. Li, and D. Viehland, "Enhancement in the field sensitivity of magnetoelectric laminate heterostructures," *Appl. Phys. Lett.*, vol. 95, art. no. 092501, Aug. 2009.
- [10] G. Harshe, "Magnetoelectric effect in piezoelectric-magnetostrictive composites," Ph.D. thesis, Dept. of Materials and Engineering, The Pennsylvania State University, University Park, PA, 1991.
- [11] M. Bichurin, V. Petrov, and G. Srinivasan, "Theory of low-frequency magnetoelectric coupling in magnetostrictive-piezoelectric bilayers," *Phys. Rev. B*, vol. 68, no. 5, art. no. 054402, 2003.
- [12] M. I. Bichurin, V. M. Petrov, and G. Srinivasan, "Theory of low-frequency magnetoelectric effects in ferromagnetic-ferroelectric layered composites," *J. Appl. Phys.*, vol. 92, pp. 7681–7683, Dec. 2002.
- [13] M. I. Bichurin, V. M. Petrov, S. V. Averkin, and E. Liverts, "Present status of theoretical modeling the magnetoelectric effect in magnetostrictive-piezoelectric nanostructures. Part I: Low frequency and electromechanical resonance ranges," *J. Appl. Phys.*, vol. 107, art. no. 053904, Mar. 2010.
- [14] C.-M. Chang and G. Carman, "Modeling shear lag and demagnetization effects in magneto-electric laminate composites," *Phys. Rev. B*, vol. 76, no. 13, art. no. 134116, 2007.
- [15] I. Osaretin and R. Rojas, "Theoretical model for the magnetoelectric effect in magnetostrictive/piezoelectric composites," *Phys. Rev. B*, vol. 82, no. 17, art. no. 174415, 2010.
- [16] Y. Wang, D. Gray, D. Berry, J. Gao, J. Li, D. Viehland, and H. Luo, "Equivalent magnetic noise in magnetoelectric Metglas/Pb(Mg $_{1/3}$ Nb $_{2/3}$ )O $_3$ -PbTiO $_3$  laminate composites," *Phys. Status Solidi Rapid Res. Lett.*, vol. 5, no. 7, pp. 232–234, 2011.
- [17] X. Zhuang, M. L. C. Sing, C. Cordier, S. Saez, C. Dolabdjian, J. Das, J. Gao, J. Li, and D. Viehland, "Analysis of noise in magnetoelectric thin-layer composites used as magnetic sensors," *IEEE Sens. J.*, vol. 11, pp. 2183–2188, Oct. 2011.
- [18] Z. Fang, N. Mokhariwale, F. Li, S. Datta, and Q. M. Zhang, "Magnetoelectric sensors with directly integrated charge sensitive readout circuit-improved field sensitivity and signal-to-noise ratio," *IEEE Sens. J.*, vol. 11, pp. 2260–2265, Oct. 2011.
- [19] R. Jahns, H. Greve, E. Woltermann, E. Quandt, and R. H. Knoechel, "Noise performance of magnetometers with resonant thin-film magnetoelectric sensors," *IEEE Trans. Instrum. Meas.*, vol. 60, pp. 2995–3001, Aug. 2011.
- [20] C. R. Bowen, L. J. Nelson, R. Stevens, M. G. Cain, and M. Stewart, "Optimisation of interdigitated electrodes for piezoelectric actuators and active fibre composites," *J. Electroceram.*, vol. 16, no. 4, pp. 263–269, 2006.
- [21] J. Gao, Y. Wang, M. Li, Y. Shen, J. Li, and D. Viehland, "Quasi-static ( $f < 10$ –2 Hz) frequency response of magnetoelectric composites based magnetic sensor," *Mater. Lett.*, vol. 85, pp. 84–87, Oct. 2012.
- [22] F. Fang, C. Zhao, and W. Yang, "Thickness effects on magnetoelectric coupling for Metglas/PZT/Metglas laminates," *Sci. China—Phys. Mech. Astron.*, vol. 54, pp. 581–585, Apr. 2011.



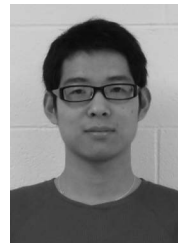
**Yaojin Wang** is a Postdoctoral Associate in the Department of Materials Science and Engineering at Virginia Tech. He received the Ph.D. degree from the Shanghai Institute of Ceramics, Chinese Academy of Science, in 2010. From March 2007 through June 2008, he worked as a Research Assistant in the Department of Applied Physics at the Hong Kong Polytechnic University (PolyU), and from June 2008 through September 2008, he worked as a Research Assistant in the Department of Electrical Engineering at PolyU.

His current research interests cover structure and properties of ferroelectric single crystals, and sensor/actuator materials, including magnetoelectricity, piezoelectricity, and magnetostriction. He has published more than 50 peer-reviewed journal articles.



**Davresh Hasanyan** received the Ph.D. degree in solids mechanics from Yerevan State University, Armenia. His current areas of research are composite structures; vibration and stability; computation in physical problems (FEA in boundary value problems); sensors and actuators, MEMS; multiferroic materials; fracture mechanics, fatigue damage mechanics, and crack growth modeling; and wave processes.

**Menghui Li** received the B.S. degree in material science and engineering from Tsinghua University, Beijing, China, in 2009. Currently, he is working toward the Ph.D. degree at the Department of Materials Science and Engineering, Virginia Polytechnic Institute and State University, Blacksburg, VA. His research focuses on magnetoelectric materials.



**Junqi Gao** is a Ph.D. candidate in the Materials Science and Engineering Department at the Virginia Polytechnic Institute and State University, Blacksburg, VA. He received his B.S. degree in materials science and engineering from Tsinghua University, Beijing, China, in 2008.

Currently, his research mainly focuses on magnetic sensors and energy harvesters based on magnetoelectric laminates, and low-noise charge amplifier design.



**Jiefang Li** received her Ph.D. degree in solid-state science from The Pennsylvania State University. She is currently a research professor of Materials Science and Engineering at Virginia Tech. Her research interests include ferroelectric, piezoelectric, dielectric, and magnetoelectric materials. She has been instrumental in the development and study of magnetoelectric laminate composites. Jiefang has published more than 100 peer-reviewed journal articles.



**Dwight Viehland** is currently in the Department of Materials Science and Engineering at Virginia Tech. He received B.S. and M.S. degrees from the University of Missouri-Rolla, and a Ph.D. degree from The Pennsylvania State University. Dwight is an experimental solid-state scientist in the structure and properties of condensed matter and thin layers. His research focuses on sensor materials, including magnetoelectricity, piezoelectricity, and magnetostriction. Since joining Virginia Tech, the Viehland laboratory began a new area of research that involved the development of novel materials/composites with large magneto-electric exchanges.